Supporting Information

Nano-architected GaN Spinodoid Metamaterials with Tailorable Anisotropic Piezoelectric Properties

Jun Cai, Alireza Seyedkanani, Benyamin Shahryari, *Zhengshu Yan, Pengxu Lu, Valérie Orsat*, and *Abdolhamid Akbarzadeh* *

J. Cai, A. Seyedkanani, B. Shahryari, P. Lu, Prof. V. Orsat, Prof. A.H. Akbarzadeh
Department of Bioresource Engineering
McGill University
Montreal, QC H9X 3V9, Canada
* Email: hamid.akbarzadeh@mcgill.ca

Z. Yan, Prof. A.H. Akbarzadeh
Department of Mechanical Engineering
McGill University
Montreal, QC H9A 0C3, Canada

S1. Supporting Figures and Tables.

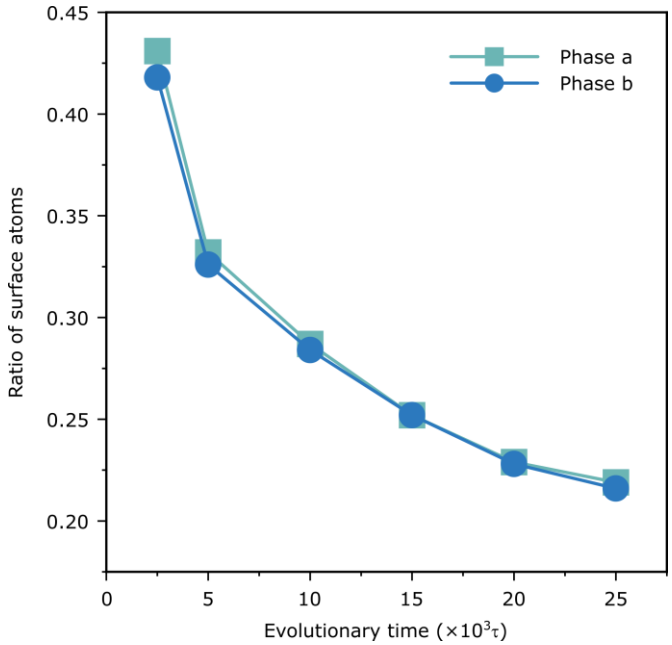

Figure S1. Ratio of surface atoms of GaN spinodoid metamaterials as a function of evolutionary time.

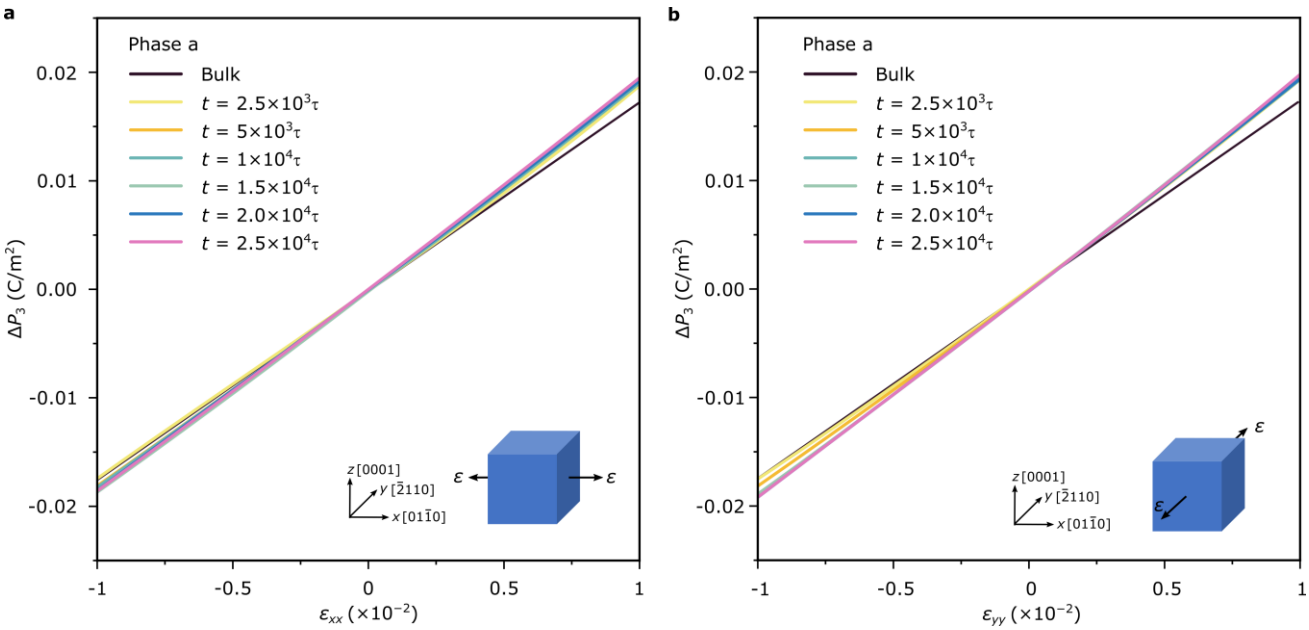

Figure S2. The change of the polarization (ΔP_3) of GaN spinodoid metamaterials (phase a) at different evolutionary times and bulk GaN as a function of mechanical strain, where external normal strains are applied along the **(a)** $[01\bar{1}0]$ and **(b)** $[\bar{2}110]$ directions, respectively.

Table S1. Piezoelectric stress constants of Wurtzite bulk GaN

	This work	MD	DFT	Experiment
e_{33} (C/m^2)	0.895	0.69 [1], 0.723 [2], 0.772 [2], 0.80 [3], 0.81[4], 1.06 [5], 1.28 [6]	0.554 [7], 0.63 [8], 0.67 [9], 0.73 [10], 0.74 [11], 0.75 [12], 0.78 [13], 0.83 [14], 0.86 [9], 1.02 [15], 1.05 [16]	1.12 [17], 1.15 ± 0.05 [18]
e_{31} (C/m^2)	-0.422	–	–0.32 [8], –0.34 [9], –0.37 [9], –0.42 [13], –0.44 [9], –0.45 [14], –0.47 [9], –0.49 [10,19], –0.551[15], –0.55 [16]	–0.14 ± 0.02 [18], –0.55 [17]

Table S2. Piezoelectric strain constants of Wurtzite GaN

	This work	Literature (Experiment and DFT)
d_{33} (pm/V)	3.605	2.0 [20], 2.13 [21], 2.7 [22], 3.1 [21,23], 3.7 [17]
d_{31} (pm/V)	–1.793	–1.4 [22], –1.9 [17]

Table S3. Elastic constants of Wurtzite GaN

	This work	Wright [24]	Polian et al. [25]
C_{11} (GPa)	353.58	367	390 ± 15
C_{12} (GPa)	139.93	135	145 ± 20
C_{13} (GPa)	123.89	103	106 ± 20
C_{33} (GPa)	369.53	405	398 ± 20
C_{44} (GPa)	97.18	95	105 ± 10

Table S4. Elastic constants of bulk GaN and GaN metamaterials (phase a) at different evolutionary times.

	C_{11}	C_{22}	C_{12}	C_{13}	C_{23}	C_{33}	C_{44}	C_{55}	C_{66}
2500τ	63.89	30.88	14.54	19.24	13.98	70.60	14.97	22.20	15.39
5000τ	75.36	29.49	15.22	19.97	14.36	70.21	14.36	23.79	16.30
10000τ	78.72	39.07	15.99	20.24	14.52	79.97	17.42	27.11	18.76
15000τ	70.99	39.22	16.44	18.98	15.36	76.73	17.76	22.97	17.52
20000τ	75.78	40.19	17.92	22.07	17.84	87.29	20.33	29.24	20.43
25000τ	80.52	43.20	17.59	21.86	18.42	87.92	20.65	31.00	22.37
Bulk	353.58	353.59	139.93	123.89	123.88	369.53	97.18	97.15	106.83

Table S5. Elastic constants of bulk GaN and GaN metamaterials (phase b) at different evolutionary times.

	C_{11}	C_{22}	C_{12}	C_{13}	C_{23}	C_{33}	C_{44}	C_{55}	C_{66}
2500τ	51.01	20.33	9.84	14.23	9.34	54.81	11.42	17.57	11.89
5000τ	61.98	18.72	9.98	15.02	7.53	56.77	9.62	20.26	12.44
10000τ	67.51	29.35	14.86	18.42	12.12	67.03	12.28	20.59	15.31
15000τ	71.52	41.93	13.26	16.79	15.86	78.64	20.36	26.60	20.21
20000τ	68.54	32.22	14.06	17.86	14.53	77.98	18.98	26.95	18.74
25000τ	75.36	41.99	12.57	16.67	14.83	90.67	23.41	29.44	23.02
Bulk	353.58	353.59	139.93	123.89	123.88	369.53	97.18	97.15	106.83

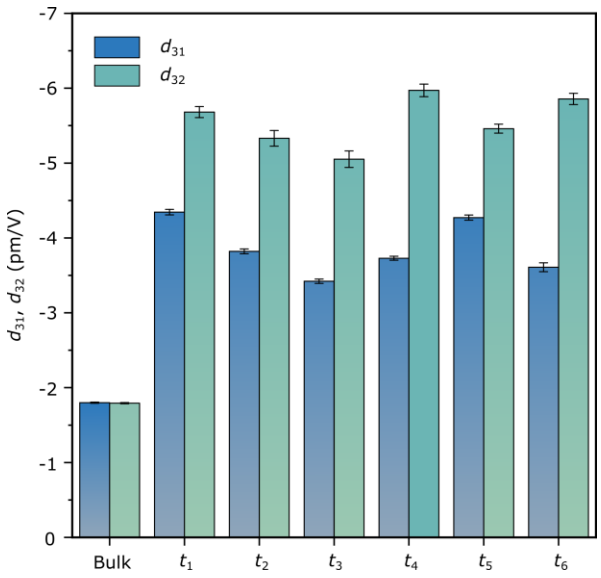

Figure S3. Piezoelectric strain constants (d_{31}, d_{32}) of bulk GaN and GaN metamaterials at different evolutionary times.

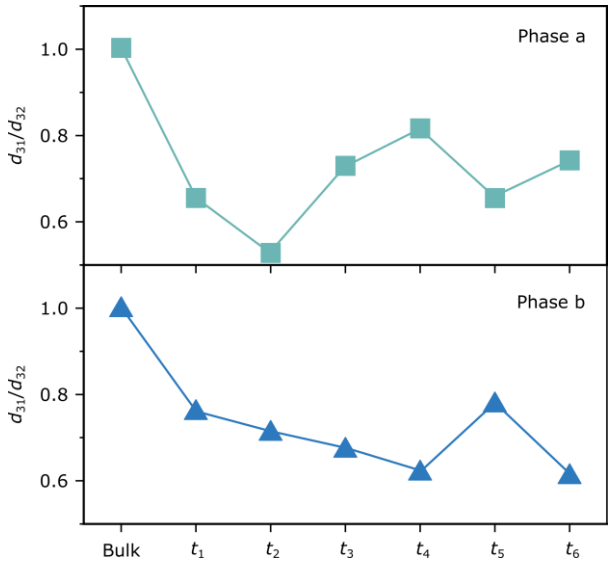

Figure S4. The ratio between d_{31} and d_{32} for bulk GaN and GaN spinodoid metamaterials at different evolutionary times.

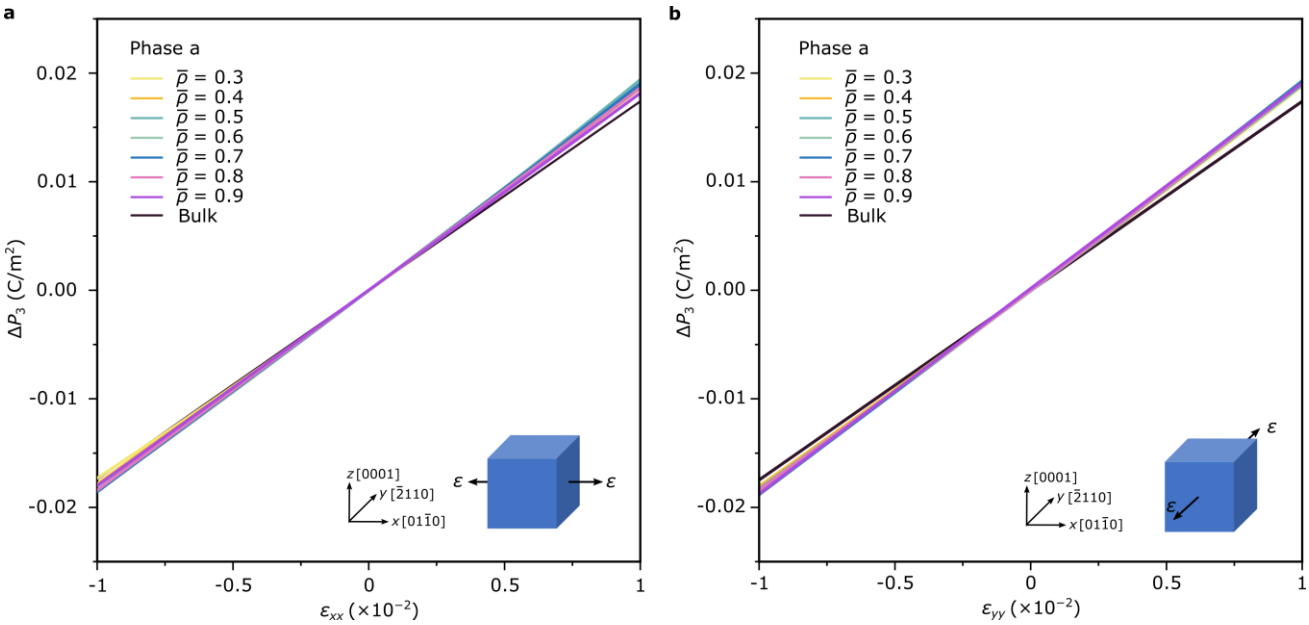

Figure S5. The change of the polarization (ΔP_3) of GaN spinodoid metamaterials (phase a) characterized by different relative densities and bulk GaN as a function of mechanical strain, where external normal strains are applied along the **(a)** [01$\bar{1}$0] and **(b)** [$\bar{2}$110] directions, respectively.

Table S6. Elastic constants of bulk GaN and GaN metamaterials (phase a) with different relative densities.

	C_{11}	C_{22}	C_{12}	C_{13}	C_{23}	C_{33}	C_{44}	C_{55}	C_{66}
0.3	22.78	6.21	4.21	7.74	3.71	22.43	3.92	6.68	4.36
0.4	47.66	20.58	9.18	13.78	9.55	45.99	9.34	13.91	9.73
0.5	75.36	29.49	15.22	19.97	14.36	70.21	14.36	23.79	16.30
0.6	110.31	57.35	23.14	27.44	21.94	100.99	25.34	34.88	27.42
0.7	143.21	106.01	36.901	37.83	33.32	149.91	39.24	46.73	41.91
0.8	191.82	119.21	48.52	53.80	43.68	190.98	47.84	58.66	52.03
0.9	253.47	206.32	80.48	79.97	71.89	270.21	69.14	75.97	74.49
Bulk	353.58	353.59	139.93	123.89	123.88	369.53	97.18	97.15	106.83

Table S7. Elastic constants of bulk GaN and GaN metamaterials (phase b) with different relative densities.

	C_{11}	C_{22}	C_{12}	C_{13}	C_{23}	C_{33}	C_{44}	C_{55}	C_{66}
0.3	9.01	1.12	1.21	2.43	0.93	5.89	0.89	2.19	1.03
0.4	13.97	5.15	1.89	4.48	1.39	13.05	2.54	4.39	2.91
0.5	61.98	18.72	9.98	15.02	7.53	56.77	9.62	20.26	12.44
0.6	61.98	18.72	9.98	15.02	7.53	56.76	9.61	20.25	12.44
0.7	88.14	42.82	16.19	21.72	15.02	88.79	19.33	27.20	20.20
0.8	114.31	56.92	25.53	32.35	22.79	115.86	28.94	38.61	34.97
0.9	170.60	113.93	44.03	49.44	39.77	187.69	45.95	56.22	48.21
Bulk	353.58	353.59	139.93	123.89	123.88	369.53	97.18	97.15	106.83

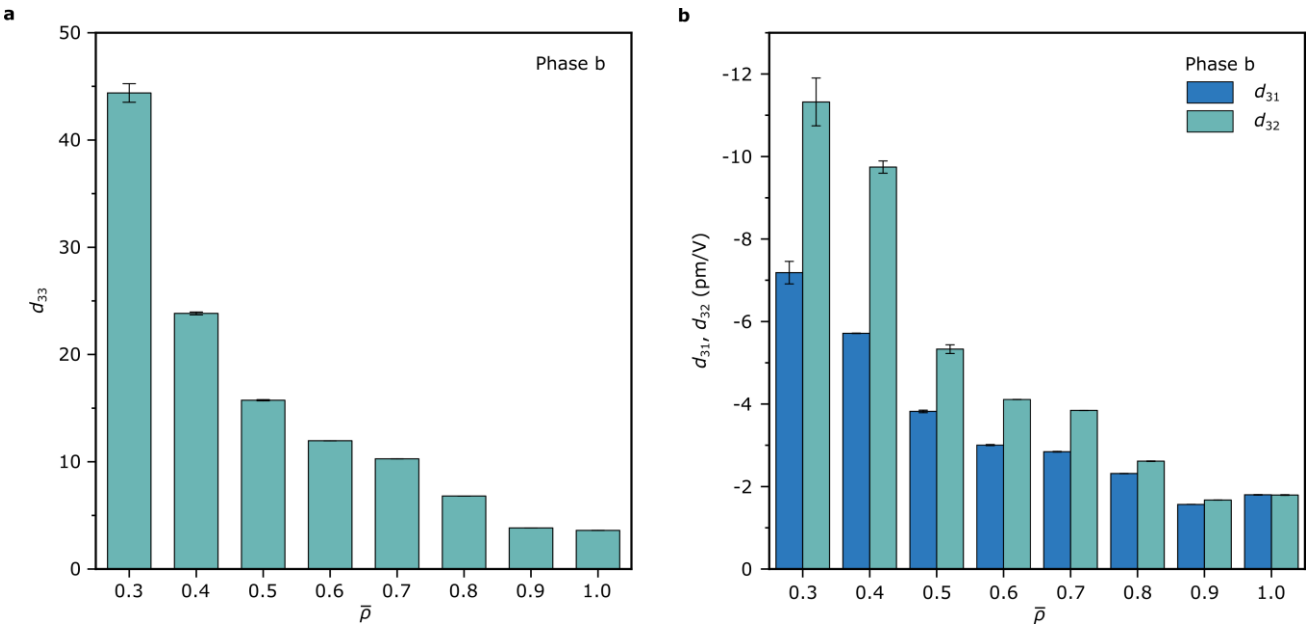

Figure S6. (a) d_{33} and **(b)** d_{31} and d_{32} of GaN spinodoid metamaterials (phase b) characterized by different relative densities. $\bar{\rho} = 1$ represents bulk GaN.

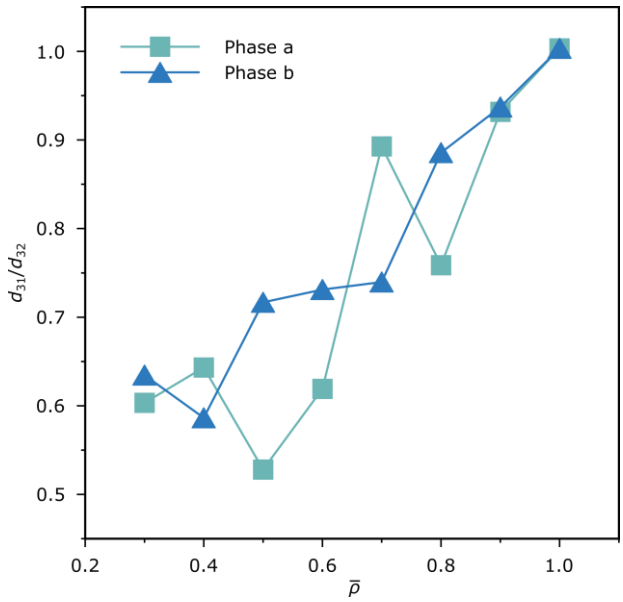

Figure S7. The ratio between d_{31} and d_{32} for GaN spinodoid metamaterials characterized by different relative densities. $\bar{\rho} = 1$ represents bulk GaN.

Table S8. Mechanical properties of bulk GaN and GaN metamaterials (phase a) with different relative densities.

	$[01\bar{1}0]$		$[\bar{2}110]$		$[0001]$	
$\bar{\rho}$	E (GPa)	σ (GPa)	E (GPa)	σ (GPa)	E (GPa)	σ (GPa)
0.3	19.94	1.62	5.59	0.87	20.68	1.60
0.4	39.35	3.15	15.9	1.38	37.41	3.21
0.5	62.59	5.34	22.71	2.33	58.16	4.95
0.6	89.76	7.75	42.56	3.88	82.65	6.29
0.7	115.14	9.73	81.97	7.50	124.63	9.33
0.8	158.74	13.07	97.64	8.89	164.53	13.19
0.9	203.87	18.03	163.04	14.34	228.69	18.12
Bulk	271.69	50.25	262.09	49.19	299.61	57.32

Table S9. Mechanical properties of bulk GaN and GaN metamaterials (phase b) with different relative densities.

	$[01\bar{1}0]$		$[\bar{2}110]$		$[0001]$	
$\bar{\rho}$	E (GPa)	σ (GPa)	E (GPa)	σ (GPa)	E (GPa)	σ (GPa)
0.3	14.53	1.25	5.66	0.66	13.56	1.02
0.4	35.23	2.84	10.55	1.47	30.22	2.65
0.5	55.22	4.87	17.79	1.83	52.66	4.67
0.6	76.55	6.55	35.49	2.82	77.87	6.07
0.7	98.71	7.80	52.98	4.71	102.58	7.61
0.8	139.29	10.80	90.48	7.40	159.41	10.93
0.9	192.01	16.20	148.79	12.66	226.59	17.09
Bulk	271.69	50.25	262.09	49.19	299.61	57.32

S2. Theoretical calcualtion of piezoelectric strian constants

$$d_{33} = \frac{C_{11}C_{22}e_{33} - C_{11}C_{23}e_{32} - C_{12}^2e_{33} + C_{12}C_{13}e_{32} + C_{12}C_{23}e_{31} - C_{13}C_{22}e_{31}}{C_{11}C_{22}C_{33} - C_{11}C_{23}^2 - C_{12}^2C_{33} + 2C_{12}C_{13}C_{23} - C_{13}^2C_{22}} \quad \text{(S1)}$$

$$d_{31} = \frac{C_{12}C_{23}e_{33} - C_{12}C_{33}e_{32} - C_{13}C_{22}e_{33} + C_{13}C_{23}e_{32} + C_{22}C_{33}e_{31} - C_{23}^2e_{31}}{C_{11}C_{22}C_{33} - C_{11}C_{23}^2 - C_{12}^2C_{33} + 2C_{12}C_{13}C_{23} - C_{13}^2C_{22}} \quad \text{(S2)}$$

$$d_{32} = \frac{-C_{11}C_{23}e_{33} + C_{11}C_{33}e_{32} + C_{12}C_{13}e_{33} - C_{12}C_{33}e_{31} - C_{13}^2e_{32} + C_{13}C_{23}e_{31}}{C_{11}C_{22}C_{33} - C_{11}C_{23}^2 - C_{12}^2C_{33} + 2C_{12}C_{13}C_{23} - C_{13}^2C_{22}} \quad \text{(S3)}$$

S3. Universal anisotropy index (A_U)

To characterize the elastic anisotropy of GaN spinodoid metamaterials, the universal anisotropy index (A_U) is applied, which is given by [26]:

$$A_U = 5\frac{G_V}{G_R} + \frac{B_V}{B_R} - 6 \quad \text{(S4)}$$

where G_V, G_R, B_V, and B_R represent the Voigt shear modulus, Reuss shear modulus, Voigt bulk modulus, and Reuss bulk modulus. G_V, G_R, B_V, and B_R are given by [27]:

$$G_V = \frac{(c_{11}+c_{22}+c_{33}) - (c_{23}+c_{13}+c_{12}) + 3(c_{44}+c_{55}+c_{66})}{15} \quad \text{(S5)}$$

$$G_R = \frac{15}{4(s_{11}+s_{22}+s_{33}) - 4(s_{23}+s_{13}+s_{12}) + 3(s_{44}+s_{55}+s_{66})} \quad \text{(S6)}$$

$$B_V = \frac{(c_{11}+c_{22}+c_{33}) + 2(c_{23}+c_{13}+c_{12})}{9} \quad \text{(S7)}$$

$$B_R = \frac{1}{(s_{11}+s_{22}+s_{33}) + 2(s_{23}+s_{13}+s_{12})} \quad \text{(S8)}$$

where c_{ij} and s_{ij} represent the ealstic cosntnats of stiffness tensor and components of the compliance tensor.

S4. Topology-dependent mechanical property

The reduced stiffness, ultimate tensile strength, and failure strain of GaN spinodoid metamaterials compared to bulk GaN originate from a combination of porosity, surface effects, and topology-induced stress concentration [28-31], all of which are intrinsic to the spinodoid architecture.

First, the introduction of a porous spinodoid topology significantly reduces the effective load-bearing cross-sectional area. Under mechanical loading, stresses are concentrated within the thin ligaments and struts of the spinodoid network, leading to reduced effective stiffness and strength compared to bulk GaN. This effect becomes more pronounced at lower relative densities, where ligament slenderness increases. From a theoretical perspective, this mechanical response is consistent with the Hashin-Shtrikman (HS) bounds theory [32], which provides theoretical upper and lower bounds for the effective stiffness of multiphase materials with arbitrary phase geometries. Treating GaN as the solid phase and air as the void phase, the HS and Suquet upper (SU) bonds for stiffness and ultimate strength of architected metamaterials can be given as [32-35]:

$$E_{HS}^{+} = \frac{2(\rho/\rho_0)\times(5v-7)}{\sqrt{13\left(\frac{\rho}{\rho_0}\right)+12v_0-2\left(\frac{\rho}{\rho_0}\right)v-15\left(\frac{\rho}{\rho_0}\right)v_0{}^2+15v_0{}^2-27}}E_0 \tag{S9}$$

$$\sigma_{SU}^{+} = \frac{2(\rho/\rho_0)}{\sqrt{4+\frac{11}{3}(1-\rho/\rho_0)}}\sigma_0 \tag{S10}$$

where E_{HS}^{+} and σ_{HS}^{+} represent the upper HS bounds for the stiffness and ultimate strength of the architected metamaterials. E_0, σ_0, and v_0 represent Young's modulus, ultimate strength, and Poisson's ratio of bulk GaN, respectively. These expressions show that stiffness and strength decrease nonlinearly with decreasing relative density, explaining why GaN spinodoid metamaterials exhibit reduced mechanical properties compared to bulk GaN.

Second, the large fraction of free surface atoms in spinodoid metamaterials further weakens mechanical performance. The nanoscale surface effect depends on both crystallographic orientation and surface-to-volume ratio, and becomes more significant at lower relative densities [28].

Third, the asymmetric topological design of the spinodoid metamaterials breaks the in-plane geometric symmetry, leading to direction-dependent and nonuniform stress distribution. While the overall reduction in stiffness and strength is primarily governed by porosity and surface effects, the asymmetric topology gives rise to anisotropic elastic responses, manifested as different mechanical behaviors along the $[01\bar{1}0]$ and $[\bar{2}110]$ directions. However, such topology design also contributes to localized stress concentrations (Figure 6b in the manuscript), leading to the reduced failure strain compared to bulk GaN.

Importantly, reduced mechanical properties are a general feature of porous architected materials and are not unique to asymmetric topologies. Symmetric architectures, such as triply periodic minimal

surface (TPMS) structures [28], also exhibit decreased stiffness and strength compared to bulk GaN due to porosity and surface effects. However, different from symmetric topologies, the asymmetric spinodoid design uniquely introduces elastic anisotropy, which plays a critical role in enabling the direction-dependent piezoelectric and mechanical responses reported in this work.

S5. Manufacturing feasibility

Here we outline two potential fabrication strategies for GaN spinodoid metamateirals. One potential route is two-photon lithography (TPL) with negative-tone photoresists such as IP-Dip [36,37], which enables fully three-dimensional, free-form polymer spinodoid templates with precise control over topology and connectivity [38-40]. These polymer architectures can subsequently be conformally coated with GaN using plasma-enhanced atomic layer deposition (PE-ALD) or low-temperature metal-organic chemical vapor deposition (MOCVD) [41], followed by template removal via thermal decomposition or solvent-based dissolution to yield hollow GaN networks. Atomic layer deposition (ALD) is particularly well suited for coating complex, high-aspect-ratio architectures due to its excellent conformality and nanometer-scale thickness control.

An alternative route is **directed self-assembly (DSA)**. Block copolymers can be thermally or solvent annealed to form bicontinuous, spinodal-like morphologies. DSA strategies, including graphoepitaxy and chemically patterned substrates, can be employed to improve long-range order and orientation [42]. Selective removal of one polymer phase results in a nanoporous three-dimensional template with characteristic length scales in the 10-50 nm range [43,44]. GaN can then be deposited into or onto the template using atomic layer deposition or selective-area epitaxy, yielding either solid or hollow spinodoid networks depending on the process. Removal of residual polymer produces freestanding or substrate-supported GaN architectures.

In the present work, the characteristic length scale of the spinodoid architecture is approximately $L \approx 20$ nm, corresponding to ligament thicknesses of only a few nanometers at low relative densities. While experimentally challenging, this length scale lies within or near the lower bound of current nanofabrication capabilities. In particular, block copolymer self-assembly routinely yields bicontinuous morphologies with characteristic dimensions in the 10-50 nm range, making it well matched to the length scales considered in this study. When combined with conformal deposition techniques such as atomic layer deposition, effective GaN ligament thicknesses of only a few nanometers are experimentally attainable. In contrast, two-photon lithography offers unmatched geometric freedom for three-dimensional architectures but typically produces feature sizes in the range of 50-200 nm, making it challenging to fabricate the GaN spinodoid metamaterials explored in current study.

While the primary focus of this study is computational, we explicitly acknowledge experimental challenges to achieve ultralight, 3D GaN spinodoid metamaterials. Particularly, achieving nanometer-scale ligament thicknesses in bicontinuous GaN networks requires precise control over deposition uniformity, crystallinity, and residual stresses, especially when conformal coating or template-inversion approaches are employed [45]. The brittle nature of GaN further increases the susceptibility of low-density architectures to damage during template removal, handling, and characterization. Moreover, establishing reliable electrical contacts and performing quantitative piezoelectric measurements on highly porous three-dimensional geometries remain challenging tasks.

S6. Additional results

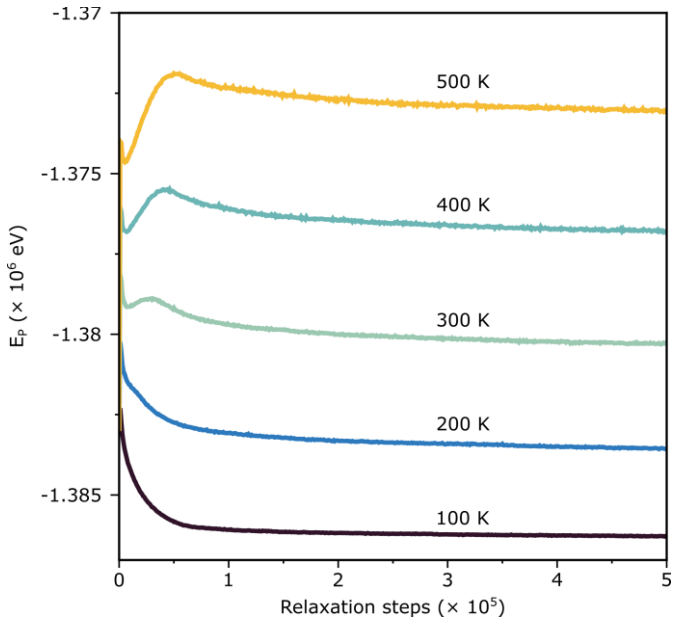

Figure S8. Evaluation of potential energy of GaN Spinodoid metamaterials ($t = 10000\tau$, $L \approx 20$ nm, and $\bar{\rho} = \rho/\rho_0 \approx 0.5$) as a function of relaxation steps.

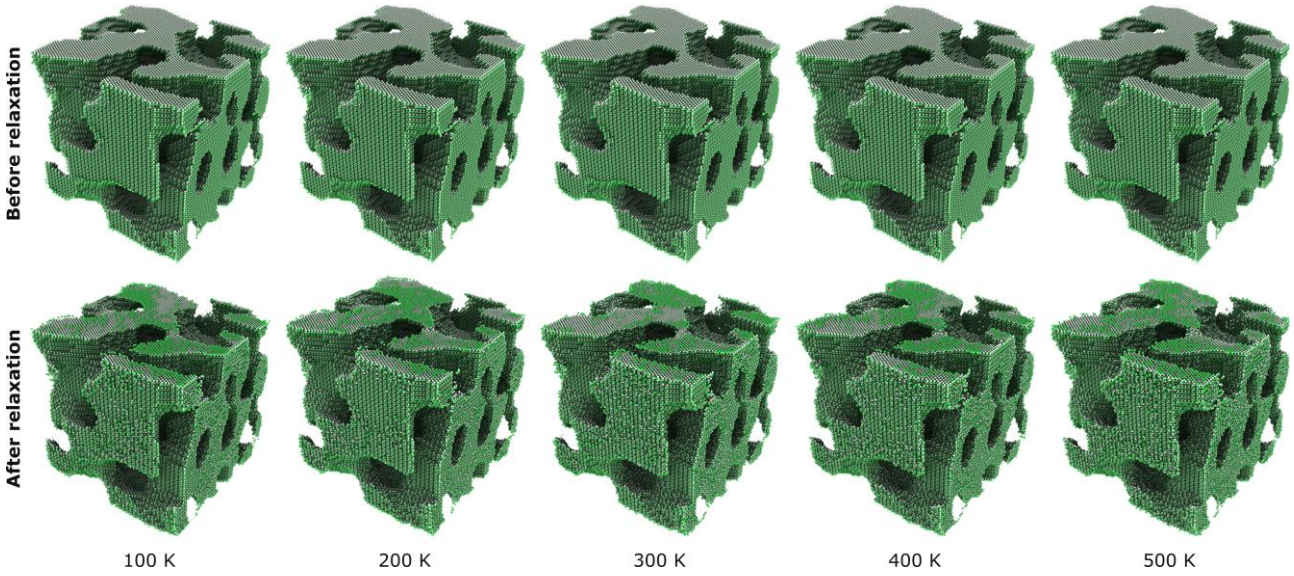

Figure S9. GaN spinodoid metamaterial ($t = 10000\tau$, $L \approx 20$ nm, and $\bar{\rho} = \rho/\rho_0 \approx 0.5$) before and after structural relaxation in MD simulations at different temperatures (100-500 K). The topologies remain unchanged after relaxation, confirming the thermal stability of the spinodoid architecture.

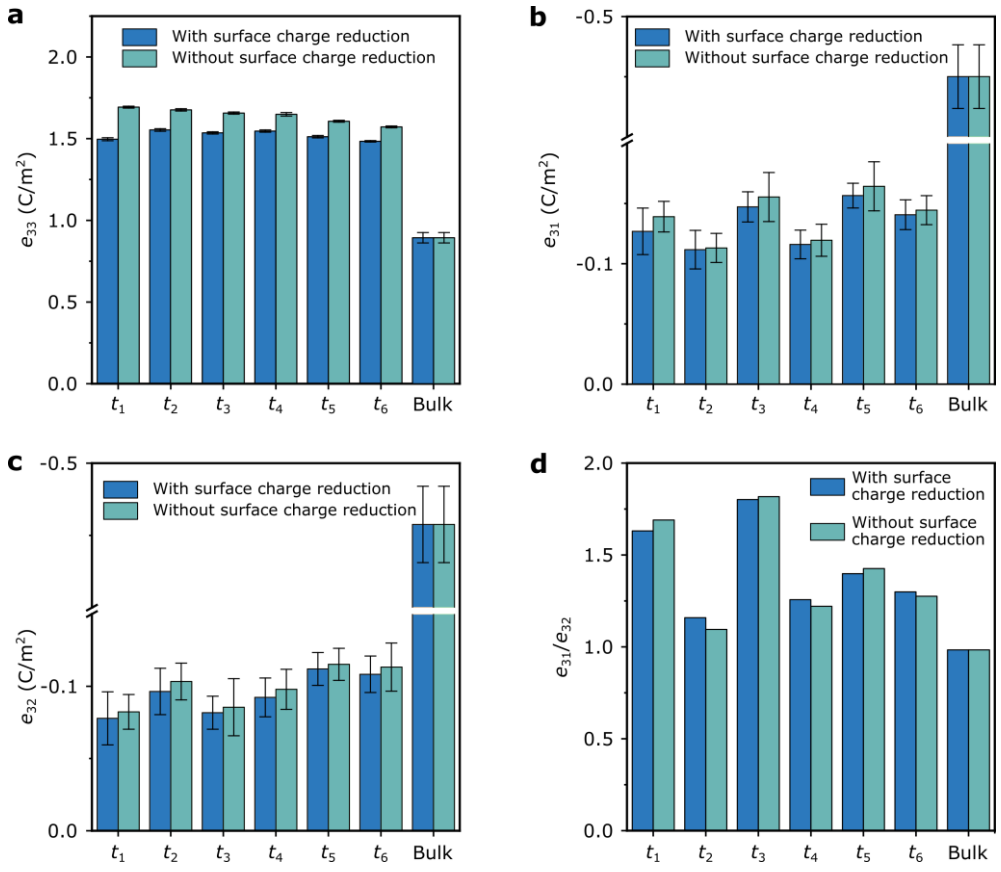

Figure S10. (a) e_{33}, **(b)** e_{31}, and **(c)** e_{32} of bulk GaN and GaN spinodoid metamateirals at different evolutionary times (t_1, t_2, t_3, t_4, t_5, and t_6 correspond to 2500τ, 5000τ, 10000τ, 15000τ, 20000τ, and 25000τ, respectively. τ = 0.015) with/without considering the reduced partial charges of surface atoms. Since bulk GaN does not contain any surface atoms, the two values of piezoelectric stress constants are identical for bulk GaN. **(d)** The ratio between e_{31} and e_{32} for bulk GaN and GaN spinodoid metamaterials at different evolutionary times with/without considering the reduced partial charges of surface atoms.

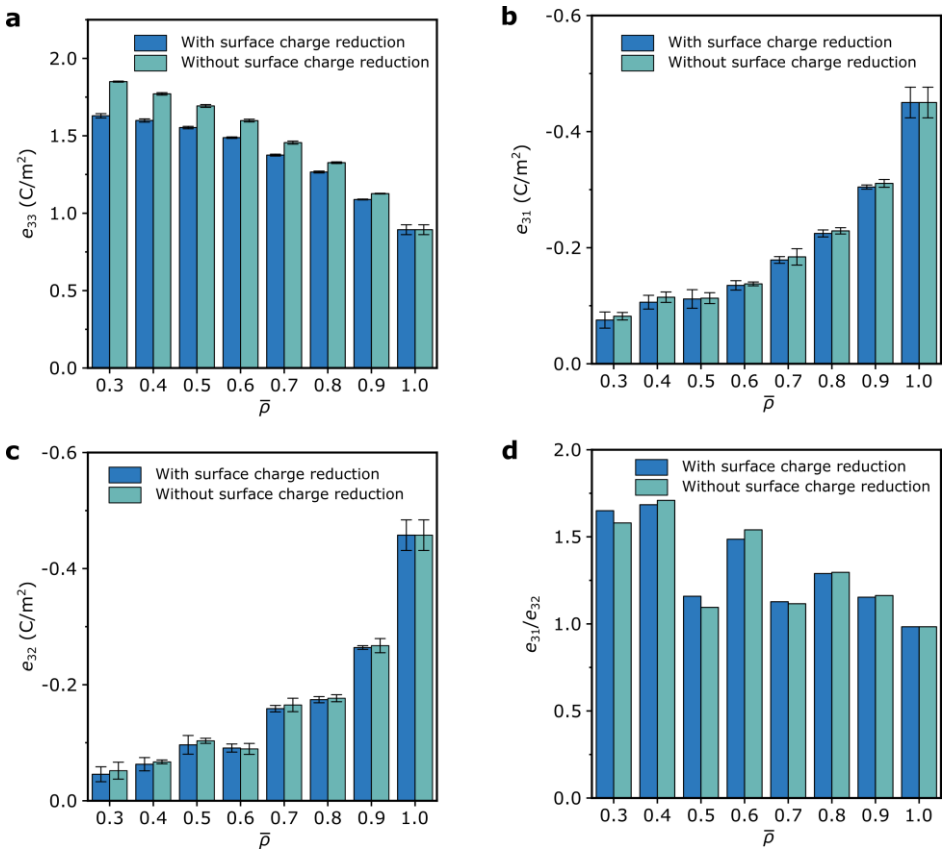

Figure S11. (a) e_{33}, **(b)** e_{31}, and **(c)** e_{32} of bulk GaN and GaN spinodoid metamateirals characterized by different relative densities with/without considering the reduced partial charges of surface atoms. Since bulk GaN does not contain any surface atoms, the two values of piezoelectric stress constants are identical for bulk GaN. **(d)** The ratio between e_{31} and e_{32} for bulk GaN and GaN spinodoid metamaterials characterized by different relative densities with/without considering the reduced partial charges of surface atoms.

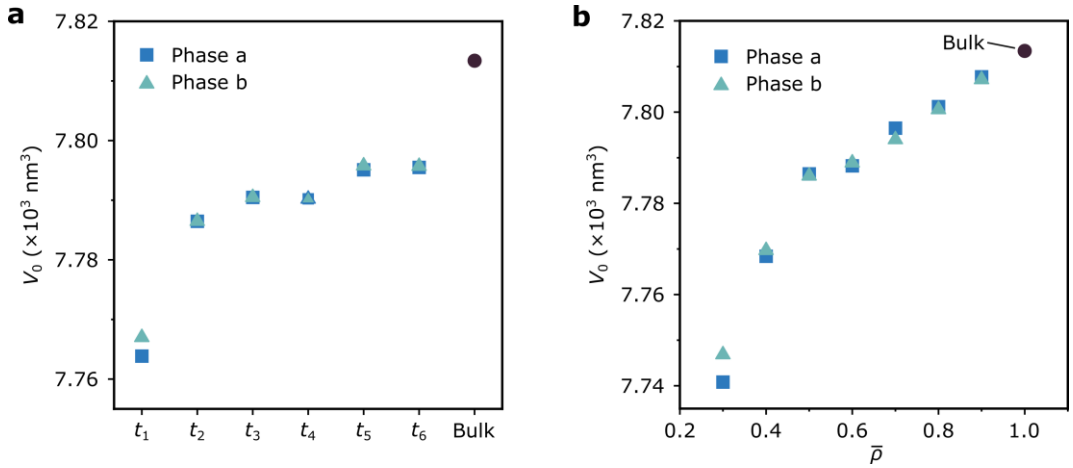

Figure S12. The cubic volume of the GaN metamaterials characterized by **(a)** different evolutionary times and **(b)** different relative densities after a full relaxation in MD simulation. The volume of GaN metamaterials is reduced compared to that of bulk GaN

To better understand the role of the free surfaces in the piezoelectric metamateirals, **we first analyze their charge density difference distribution** using first-principals calculations based on DFT. The calculations utilize a projector augmented wave (PAW) pseudopotential [46], and employ the Perdew-Burke-Ernzerh (PBE) method [47] to describe the exchange-correlation energy functional. The wave cut-off energy for both valence electrons and ion cores is set at 500 eV to ensure precise calculations across various electronic and structural configurations [48]. Additionally, stringent convergence criteria are set at 10^{-3} eV/Å for force and 10^{-5} eV for energy during structural relaxation to guarantee the accuracy and reliability of computational results. The geometry optimization of the piezo-structure and the charge density calculations of bulk GaN are performed within the framework of a periodic infinite crystal. To gain molecular-level insights into surface effects, the analysis is extended to non-periodic piezo-structures. A substantial vacuum layer of 15 Å is implemented to effectively isolate upper and lower surface atoms to eliminate undesired interactions. The convergence criteria for this non-periodic piezo-structure are consistent with those employed in the bulk models. Figure S13a compares the charge density difference distributions of bulk GaN and GaN nanostructures with representative free surfaces $(01\bar{1}0)$, $(2\bar{1}\bar{1}0)$, and (0001), corresponding to the crystallographic planes normal to the *x*-, *y*-, and *z*-axes in Figure. 1 in the manuscript). In bulk GaN, the charge density difference is uniformly distributed, reflecting the symmetric coordination environment. In contrast, in non-periodic structures, the charge density difference of the atoms on the free surfaces differs from that of internal atoms. The difference observed in GaN NWs arises from changes in the sp^3 hybrid orbital of electrons. Hence, in this study, we reduced the charge of the surface atoms to 75% of that of bulk atoms. This treatment captures the negative contribution of surface polarization to the piezoelectric response. Importantly, as the surface-to-volume ratio decreases, the proportion of surface atoms is reduced, thereby weakening the influence of surface polarization.

We next examine the evolution of the dielectric constant with surface-to-volume ratio. In the calculation of the dielectric constant of the GaN spinodoid metamaterials and bulk GaN, an external electric field E_i is applied while the simulation box is fixed to ensure no strain occurs in all directions. Then, the dielectric constant can be obtained by [3,49]

$$\kappa_{ij} = \left.\frac{\partial D_i}{\partial E_j}\right|_{\varepsilon=0} \tag{S11}$$

where $D_i = \kappa_0 E_i + P_i$ is the electric displacement in *i*-axis, κ_0 is the vacuum permittivity, and P_i denotes the polarization. Substituting the expression of D_i into Eq. (S11) yields

$$\kappa_{ij} = \left.\frac{\partial D_i}{\partial E_j}\right|_{\varepsilon=0} = \frac{\partial(\kappa_0 E_j + P_i)}{\partial E_j} = \kappa_0 + \frac{\partial P_i}{\partial E_j} \tag{S12}$$

Hence the relative permittivity (κ_{ij}^{r}) expressing as a ratio relative to the vacuum permittivity (κ_0) is given by

$$\kappa_{ij}^{r} = \frac{\kappa_{ij}}{\kappa_0} = 1 + \frac{1}{\kappa_0}\frac{\partial P_i}{\partial E_j} \tag{S13}$$

The calculated relative dielectric constant of bulk GaN is κ_{33}^{r} = 3.48, which is slightly smaller than the theoretical results but agrees well with the previously reported MD results (κ_{33}^{r} = 3.17 – 3.243) [50,51]. As shown in Figure S13b, the relative dielectric constant of GaN spinodoid metamaterials decreases with the increased surface-to-volume ratio.

Finally, we analyze volumetric shrinkage, defined as $(V\text{-}V_0)/V_0$, where V and V_o are the cubic volume of the GaN metamateirals and bulk GaN, respectively. Figure S13c shows that the volumetric shrinkage decreases as the surface-to-volume ratio decreases. At low surface-to-volume ratios (high relative density), the relaxed volume of the spinodoid metamaterials closely approaches that of bulk GaN, indicating weakened surface effects.

Taken together, these results demonstrate that decreasing surface-to-volume ratio weakens surface polarization effect, increases dielectric constant, and reduces volumetric shrinkage. As a result, both piezoelectric enhancement and anisotropy diminish at high relative densities. This trend explains why GaN spinodoid metamaterials with high relative density exhibit piezoelectric properties and anisotropy approaching those of bulk GaN (Figures 4d and 4e in the manuscript).

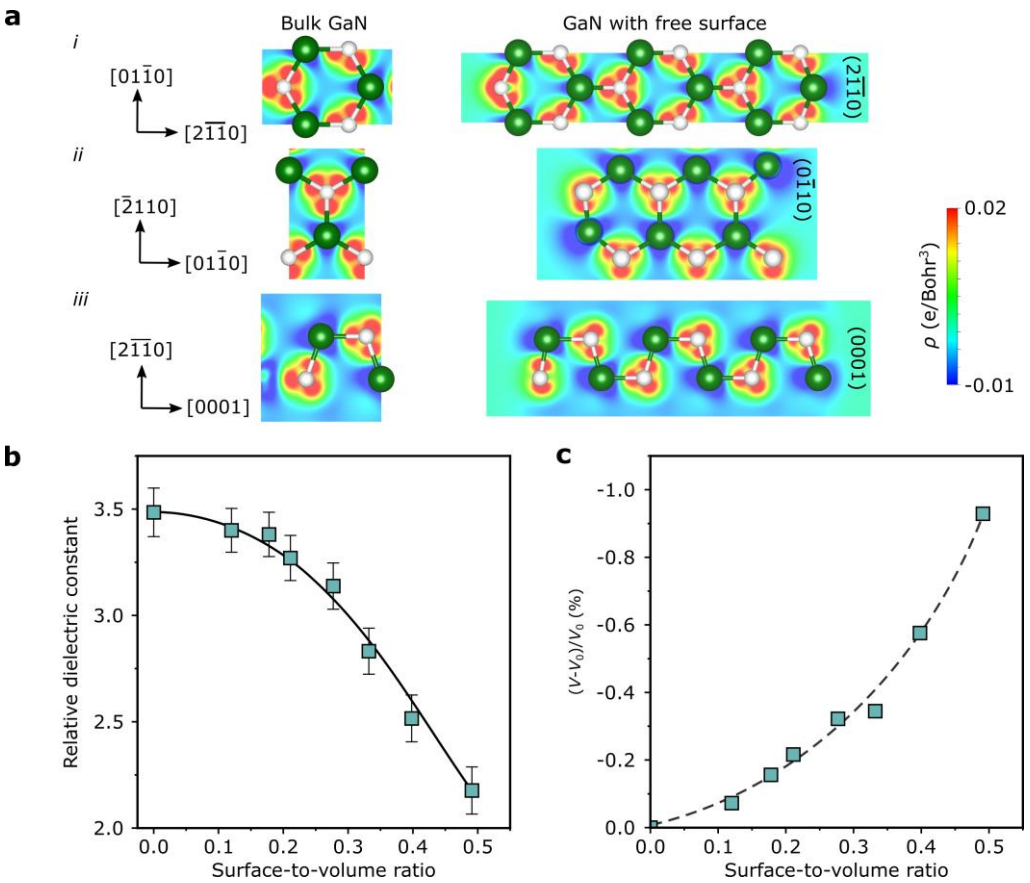

Figure S13. (a) charge density difference distribution of bulk GaN and GaN nanowires characterized by different free surfaces. **(b)** Relative dielectric constant and **(c)** volumetric shrinkage of GaN metamaterials characterized by different surface-to-volume ratios.

Reference

[1] Zhang J, Wang C, Chowdhury R, Adhikari S (2013) Size- and temperature-dependent piezoelectric properties of gallium nitride nanowires. *Scripta Materialia* **68**, 627-630 https://doi.org:10.1016/j.scriptamat.2012.12.022
[2] Zhang J, Meguid SA (2015) On the piezoelectric potential of gallium nitride nanotubes. *Nano Energy* **12**, 322-330 https://doi.org:10.1016/j.nanoen.2014.12.036
[3] Zhang J (2014) Small-scale effect on the piezoelectric potential of gallium nitride nanowires. *Applied Physics Letters* **104**, 253110 https://doi.org:10.1063/1.4885538
[4] Zhang J, Wang C (2016) Size-dependent pyroelectric properties of gallium nitride nanowires. *Journal of Applied Physics* **119**, 145102 https://doi.org:10.1063/1.4945765
[5] Zhang J (2020) On the piezotronic behaviours of wurtzite core-shell nanowires. *Nanotechnology* **31**, 095407 https://doi.org:10.1088/1361-6528/ab5881
[6] Zhang J (2021) Tunable local and global piezopotential properties of graded InGaN nanowires. *Nano Energy* **86**, 106125 https://doi.org:10.1016/j.nanoen.2021.106125
[7] Agrawal R, Espinosa HD (2011) Giant piezoelectric size effects in zinc oxide and gallium nitride nanowires. A first principles investigation. *Nano Lett* **11**, 786-790 https://doi.org:10.1021/nl104004d
[8] Shimada K, Sota T, Suzuki K (1998) First-principles study on electronic and elastic properties of BN, AlN, and GaN. *Journal of Applied Physics* **84**, 4951-4958 https://doi.org:10.1063/1.368739
[9] Zoroddu A, Bernardini F, Ruggerone P, Fiorentini V (2001) First-principles prediction of structure, energetics, formation enthalpy, elastic constants, polarization, and piezoelectric constants of AlN, GaN, and InN: Comparison of local and gradient-corrected density-functional theory. *Physical Review B* **64** https://doi.org:10.1103/PhysRevB.64.045208
[10] Bernardini F, Fiorentini V, Vanderbilt D (1997) Spontaneous polarization and piezoelectric constants of III-V nitrides. *Physical Review B* **56**, R10024-R10027 https://doi.org:10.1103/PhysRevB.56.R10024
[11] Caro MA, Schulz S, O'reilly EP (2013) Theory of local electric polarization and its relation to internal strain: Impact on polarization potential and electronic properties of group-III nitrides. *Physical Review B* **88**, 214103 https://doi.org:10.1103/PhysRevB.88.214103
[12] Prodhomme P-Y, Beya-Wakata A, Bester G (2013) Nonlinear piezoelectricity in wurtzite semiconductors. *Physical Review B* **88**, 121304
[13] Shen X-P, Lin J-B, Hu R-Y, Liu Y-C, Xu L-Q, Niu H-B, Xiao X-F, Wang V (2024) Compositional effects on structural, electronic, elastic, piezoelectric and dielectric properties of GaInN alloys: a first-principles study. *RSC advances* **14**, 6752-6761
[14] Shimada K (2006) First-Principles Determination of Piezoelectric Stress and Strain Constants of Wurtzite III–V Nitrides. *Japanese Journal of Applied Physics* **45**, L358 https://doi.org:10.1143/JJAP.45.L358
[15] Dreyer CE, Janotti A, Van De Walle CG, Vanderbilt D (2016) Correct Implementation of Polarization Constants in Wurtzite Materials and Impact on III-Nitrides. *Physical Review X* **6** https://doi.org:10.1103/PhysRevX.6.021038
[16] Pal J, Tse G, Haxha V, Migliorato MA, Tomić S (2011) Second-order piezoelectricity in wurtzite III-N semiconductors. *Physical Review B* **84**, 085211
[17] Guy IL, Muensit S, Goldys EM (1999) Extensional piezoelectric coefficients of gallium nitride and aluminum nitride. *Applied Physics Letters* **75**, 4133-4135 https://doi.org:10.1063/1.125560
[18] Adachi K, Ogi H, Nagakubo A, Nakamura N, Hirao M, Imade M, Yoshimura M, Mori Y (2016) Piezoelectric coefficients of GaN determined by hopping conduction of carriers. *Applied Physics Letters* **109** https://doi.org:10.1063/1.4966995
[19] Gaska R, Shur MS, Bykhovski AD (2014) Pyroelectric and Piezoelectric Properties of GaN-Based Materials. *MRS Internet Journal of Nitride Semiconductor Research* **4**, 57-68 https://doi.org:https://doi.org/10.1557/S1092578300002246

[20] Lueng CM, Chan HLW, Surya C, Choy CL (2000) Piezoelectric coefficient of aluminum nitride and gallium nitride. *Journal of Applied Physics* **88**, 5360-5363 https://doi.org:10.1063/1.1317244
[21] Lueng CM, Chan HLW, Surya C, Fong WK, Choy CL, Chow P, Rosamond M (1999) Piezoelectric coefficient of GaN measured by laser interferometry. *Journal of Non-Crystalline Solids* **254**, 123-127 https://doi.org:10.1016/s0022-3093(99)00383-x
[22] Muensit S, Guy IL (1998) The piezoelectric coefficient of gallium nitride thin films. *Applied Physics Letters* **72**, 1896-1898 https://doi.org:10.1063/1.121219
[23] Vurgaftman I, Meyer JR (2003) Band parameters for nitrogen-containing semiconductors. *Journal of Applied Physics* **94**, 3675-3696 https://doi.org:10.1063/1.1600519
[24] Wright AF (1997) Elastic properties of zinc-blende and wurtzite AlN, GaN, and InN. *Journal of Applied Physics* **82**, 2833-2839 https://doi.org:10.1063/1.366114
[25] Polian A, Grimsditch M, Grzegory I (1996) Elastic constants of gallium nitride. *Journal of Applied Physics* **79**, 3343-3344 https://doi.org:10.1063/1.361236
[26] Ranganathan SI, Ostoja-Starzewski M (2008) Universal elastic anisotropy index. *Phys Rev Lett* **101**, 055504 https://doi.org:10.1103/PhysRevLett.101.055504
[27] Hill R (1952) The Elastic Behaviour of a Crystalline Aggregate. *Proceedings of the Physical Society. Section A* **65**, 349-354 https://doi.org:10.1088/0370-1298/65/5/307
[28] Chen CT, Chrzan DC, Gu GX (2020) Nano-topology optimization for materials design with atom-by-atom control. *Nat Commun* **11**, 3745 https://doi.org:10.1038/s41467-020-17570-1
[29] Jung GS, Buehler MJ (2018) Multiscale Mechanics of Triply Periodic Minimal Surfaces of Three-Dimensional Graphene Foams. *Nano Lett* **18**, 4845-4853 https://doi.org:10.1021/acs.nanolett.8b01431
[30] Park JH, Lee JC (2017) Unusually high ratio of shear modulus to Young's modulus in a nano-structured gyroid metamaterial. *Sci Rep* **7**, 10533 https://doi.org:10.1038/s41598-017-10978-8
[31] Park JH, Lee JC (2019) Peculiar elastic behavior of mechanical metamaterials with various minimal surfaces. *Sci Rep* **9**, 2941 https://doi.org:10.1038/s41598-019-38660-1
[32] Hashin Z, Shtrikman S (1963) A variational approach to the theory of the elastic behaviour of multiphase materials. *Journal of the Mechanics and Physics of Solids* **11**, 127-140 https://doi.org:10.1016/0022-5096(63)90060-7
[33] Bauer J, Meza LR, Schaedler TA, Schwaiger R, Zheng X, Valdevit L (2017) Nanolattices: An Emerging Class of Mechanical Metamaterials. *Adv Mater* **29** https://doi.org:10.1002/adma.201701850
[34] Suquet PM (1993) Overall potentials and extremal surfaces of power law or ideally plastic composites. *Journal of the Mechanics and Physics of Solids* **41**, 981-1002 https://doi.org:10.1016/0022-5096(93)90051-g
[35] Crook C, Bauer J, Guell Izard A, Santos De Oliveira C, Martins De Souza ESJ, Berger JB, Valdevit L (2020) Plate-nanolattices at the theoretical limit of stiffness and strength. *Nat Commun* **11**, 1579 https://doi.org:10.1038/s41467-020-15434-2
[36] Deng W, Kumar S, Vallone A, Kochmann DM, Greer JR (2024) AI-Enabled Materials Design of Non-Periodic 3D Architectures With Predictable Direction-Dependent Elastic Properties. *Adv Mater* **36**, e2308149 https://doi.org:10.1002/adma.202308149
[37] Kumar S, Tan S, Zheng L, Kochmann DM (2020) Inverse-designed spinodoid metamaterials. *npj Computational Materials* **6**, 73 https://doi.org:10.1038/s41524-020-0341-6
[38] Geng Q, Wang D, Chen P, Chen SC (2019) Ultrafast multi-focus 3-D nano-fabrication based on two-photon polymerization. *Nat Commun* **10**, 2179 https://doi.org:10.1038/s41467-019-10249-2
[39] Harinarayana V, Shin YC (2021) Two-photon lithography for three-dimensional fabrication in micro/nanoscale regime: A comprehensive review. *Optics & Laser Technology* **142**, 107180 https://doi.org:10.1016/j.optlastec.2021.107180
[40] Jaiswal A, Rastogi CK, Rani S, Singh GP, Saxena S, Shukla S (2023) Two decades of two-photon lithography: Materials science perspective for additive manufacturing of 2D/3D nano-microstructures. *iScience* **26**, 106374 https://doi.org:10.1016/j.isci.2023.106374
[41] Dasgupta NP, Lee H-B-R, Bent SF, Weiss PS (2016) Recent Advances in Atomic Layer Deposition. *Chemistry of Materials* **28**, 1943-1947 https://doi.org:10.1021/acs.chemmater.6b00673

[42] Li W, Müller M (2016) Directed self-assembly of block copolymers by chemical or topographical guiding patterns: Optimizing molecular architecture, thin-film properties, and kinetics. *Progress in Polymer Science* **54-55**, 47-75 https://doi.org:10.1016/j.progpolymsci.2015.10.008
[43] Bita I, Yang JK, Jung YS, Ross CA, Thomas EL, Berggren KK (2008) Graphoepitaxy of self-assembled block copolymers on two-dimensional periodic patterned templates. *Science* **321**, 939-943 https://doi.org:10.1126/science.1159352
[44] Suh HS, Kim DH, Moni P, Xiong S, Ocola LE, Zaluzec NJ, Gleason KK, Nealey PF (2017) Sub-10-nm patterning via directed self-assembly of block copolymer films with a vapour-phase deposited topcoat. *Nat Nanotechnol* **12**, 575-581 https://doi.org:10.1038/nnano.2017.34
[45] Han X, Wang Y, Tian Y, Wang Y, Peng L, Pei C, Wang T, Gong J (2025) Deposition of uniform films on complex 3D objects by atomic layer deposition for plasma etch-resistant coatings. *Natl Sci Rev* **12**, nwaf247 https://doi.org:10.1093/nsr/nwaf247
[46] Torrent M, Jollet F, Bottin F, Zérah G, Gonze X (2008) Implementation of the Projector Augmented-Wave Method in the ABINIT Code: Application to the Study of Iron under Pressure. *Computational Materials Science* **42**, 337-351 https://doi.org:10.1016/j.commatsci.2007.07.020
[47] Perdew JP, Burke K, Ernzerhof M (1996) Generalized gradient approximation made simple. *Physical Review Letters* **77**, 3865-3868 https://doi.org:10.1103/PhysRevLett.77.3865
[48] Yan L, Wang M, Zhai C, Zhao L, Lin S (2020) Symmetry-Breaking Induced Anisotropic Carrier Transport and Remarkable Thermoelectric Performance in Mixed Halide Perovskites $CsPb(I_{1-x}Br_x)_3$. *ACS Applied Materials & Interfaces* **12**, 40453-40464 https://doi.org:10.1021/acsami.0c07501
[49] Zhang J (2021) Small-scale effects on the piezopotential properties of tapered gallium nitride nanowires: The synergy between surface and flexoelectric effects. *Nano Energy* **79**, 105489 https://doi.org:10.1016/j.nanoen.2020.105489
[50] Wang F, Li L, Tang H, Hu Y (2022) Effects of thickness and orientation on electromechanical properties of gallium nitride nanofilm: A multiscale insight. *Computational Materials Science* **203** https://doi.org:10.1016/j.commatsci.2021.111122
[51] Cai J, Yan L, Seyedkanani A, Orsat V, Akbarzadeh A (2024) Nano-architected GaN metamaterials with notable topology-dependent enhancement of piezoelectric energy harvesting. *Nano Energy* **129**, 109990 https://doi.org:10.1016/j.nanoen.2024.109990